A method to compensate for migration stretch to improve the resolution of amplitude variation with offset, S-impedance (Z_S), and density (ρ)

Swetal Patel[1], Francis Oyebanji[1], and Kurt J. Marfurt[1]

Abstract

Because of their improved leverage against ground roll and multiples, as well as the ability to estimate azimuthal anisotropy, wide-azimuth 3D seismic surveys routinely now are acquired over most resource plays. For a relatively shallow target, most of these surveys can be considered to be long offset as well, containing incident angles up to 45°. Unfortunately, effective use of the far-offset data often is compromised by noise and normal moveout (NMO) (or, more accurately, prestack migration) stretch. The conventional NMO correction is well-known to decrease the frequency content and distort the seismic wavelet at far offsets, sometimes giving rise to tuning effects. Most quantitative interpreters work with prestack migrated gathers rather than unmigrated NMO-corrected gathers. However, prestack migration of flat reflectors suffers from the same limitation called migration stretch. Migration stretch leads to lower S-impedance (Z_S) and density (ρ) resolution estimated from inversion, misclassification of amplitude variation with offset (AVO) types, and infidelity in amplitude variation with azimuth (AVAZ) inversion results. We have developed a matching pursuit algorithm commonly used in spectral decomposition to correct the migration stretch by scaling the stretched wavelets using a wavelet compensation factor. The method is based on hyperbolic moveout approximation. The corrected gathers show increased resolution and higher fidelity amplitudes at the far offsets leading to improvement in AVO classification. Correction for migration stretch rather than conventional "stretch-mute" corrections provides three advantages: (1) preservation of far angles required for accurate ρ inversion, (2) improvement in the vertical resolution of Z_S and ρ volumes, and (3) preservation of far angles that provide greater leverage against multiples. We apply our workflow to data acquired in the Fort Worth Basin and retain incident angles up to 42° at the Barnett Shale target. Comparing Z_P, Z_S, and ρ of the original gather and migration stretch-compensated data, we find an insignificant improvement in Z_P, but a moderate to significant improvement in resolution of Z_S and ρ. The method is valid for reservoirs that exhibit a dip of no more than 2°. Consistent improvement is observed in resolving thick beds, but the method might introduce amplitude anomalies at far offsets for tuning beds.

Introduction

The normal moveout (NMO) correction is to align nonzero offset traces with a zero offset trace, allowing the reflection events to be stacked and facilitating subsequent AVO, AVAZ, or prestack impedance inversion analysis. Prestack migration improves on NMO correction by reducing common midpoint (CMP) smear, placing dipping reflectors in a more accurate location, and properly focusing diffractions. In the time domain, NMO corrections and prestack migration usually are implemented on a sample-by-sample basis leading to distortion of the nonzero incident angle traces, in which the amount of distortion increases with increasing the source-receiver offset to depth ratio. Such distortion leads to a decrease in frequency and increased waveform interference at the farther incident angles. Such distorted gathers lead to a decrease in the resolution of inversion products and may create misleading results. The Aki and Richards' (1980) approximation to Zoeppritz's (1919) equations shows that P-impedance (Z_P), S-impedance (Z_S), and density (ρ) can be estimated from the "PP" reflected waves as a function of the incident angle (Figure 1). At near angles, the PP reflection is sensitive only to changes in Z_P. At farther angles, the PP reflection is sensitive to changes in all three parameters, Z_P, Z_S, and ρ. Because no converted waves are measured, the loss in resolution for inverted Z_S and ρ can be partially attributed to migration stretch.

As early as 1972, Buchholtz (1972) quantifies the degree of stretch with offset introduced by the NMO correction. To avoid the negative impact of stretch on the final stack, it was desirable to perform a mute on the

[1]The University of Oklahoma, School of Geosciences, Norman, Oklahoma 73019, USA. E-mail: swetal.patel@ou.edu (corresponding author); kmarfurt@ou.edu; Oyebanjifrancis@ou.edu.

Manuscript received by the Editor 18 October 2019; revised manuscript received 8 April 2020; published ahead of production 12 June 2020; published online 31 August 2020. This paper appears in *Interpretation*, Vol. 8, No. 4 (November 2020); p. T687–T699, 15 FIGS.

http://dx.doi.org/10.1190/INT-2019-0226.1.

DOI:10.1190/INT-2019-0226.1

part of the far-offset data that were unacceptably distorted. Because muting decreases the stack fold and causes a loss of information contained in the far-offset data, Rupert and Chun (1975) propose the block move sum (BMS) method to address the stretching problem without muting. In this method, the seismic data are treated as blocks and a single dynamic correction is applied to a block of data to eliminate stretching. Unfortunately, overlapping of adjacent blocks at far offsets introduced wavelet replication and discontinuities. Shatilo and Aminzadeh (2000), Brouwer (2002), and Masoomzadeh et al. (2010) improve upon Rupert and Chun's (1975) BMS technique. Hicks (2001) combines the Radon and spatial Fourier transforms to develop a new transform to remove the NMO stretch from the NMO-corrected CMP gather. Trickett (2003) discusses the shortcomings of the Hicks (2001) method and proposes an alternative method that directly generates stretch-free stacked data using an inversion process. However, this technique does not provide an NMO stretch-corrected CMP gather required for AVO analysis and prestack inversion. Hilterman and Van Schuyver (2003) develop an approach for wide-angle data based on prestack migration using event-based traveltime to correct the NMO stretch for a specified interval. The limitation with their method is that only the specified interval is truly flat in the gathers after the processing.

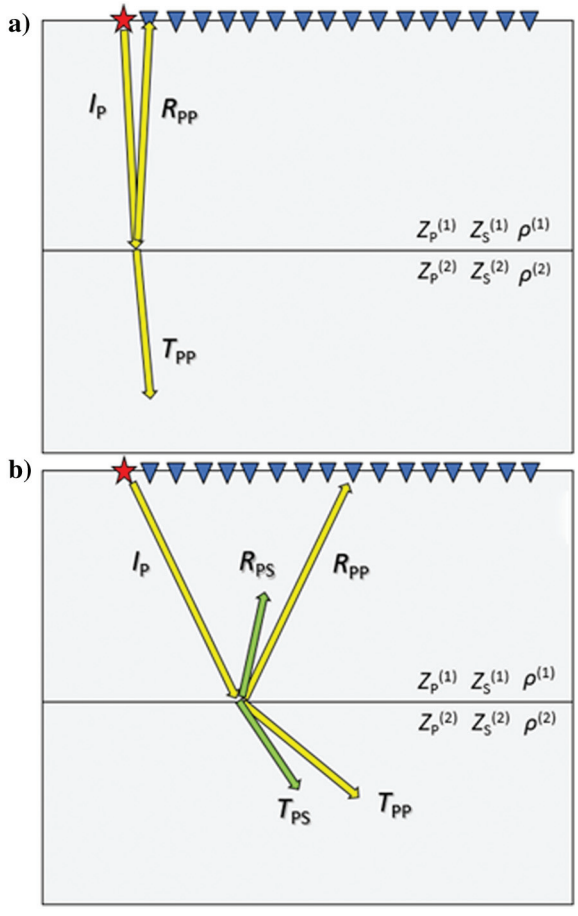

Figure 1. Diagram showing conventional PP seismic data acquisition using vertical geophones (on land) or hydrophones (at sea). (a) At near incident angles, the P-wave generates only PP reflections and transmission. Hence, the near incident angles are sensitive to only Z_P contrast across the interface. (b) At large offsets, the P-wave generates P and S reflections and transmission such that the PP reflection energy is sensitive to the Z_S and ρ contrasts across the interface as well. Because the farther offsets suffer from migration stretch, inverted for Z_S and ρ volumes often exhibit lower resolution than the corresponding Z_P volume.

Estimating the correct vertical shift of the nonzero incident angle traces for a particular reflection is the most crucial task in NMO correction. Chen et al. (2018) describe the two most common means of estimating vertical shift in NMO-correction techniques: (1) using velocities based on user-defined traveltime equations and (2) computing local time shifts of adjacent nonzero offset traces with respect to the zero offset trace (Fomel, 2007). The first technique computes the NMO correction using velocity spectra (Taner and Koehler, 1969).

Chen et al. (2018) use the second technique to align the data by applying a dynamic time wrapping (DTW) algorithm to find the time shifts based on the similarity of the adjacent traces in the prestack time-migrated gather. The process does not require a velocity spectrum; however, a velocity model is needed for the implied reverse NMO correction. The process also fails for interfering events and thin-layer waveform interference.

Careful velocity analysis is a critical tool in discriminating between primaries, reflectors, and crossing coherent events (such as multiples). Stretch correction processes developed by Perroud and Tygel (2004), Abedi and Riahi (2016), Shatilo and Aminzadeh (2000), Zhang et al. (2013), Faccipieri et al. (2019), and Abedi et al. (2019) require velocity or traveltime analysis prior to the application of the process. Zhang et al. (2013) compute a wavelet-by-wavelet rather than sample-by-sample NMO correction, in which the reflection events are modeled using a matching-pursuit wavelet-based decomposition algorithm. Mutlu and Marfurt (2015) use the workflow described by Zhang et al. (2013) and, combined with prestack structure-oriented filtering, provide S- impedance volumes exhibiting the same vertical resolution as the P-impedance volumes. The major drawbacks of the Zhang et al. (2013) algorithm are the complexity and computational intensity.

In this paper, we combine Zhang et al.'s (2013) reverse NMO and nonstretch NMO processes into one, significantly decreasing the algorithmic complexity and increasing the speed. For the same data set, Zhang et al.'s (2013) methods completed the processes of reverse NMO and nonstretch NMO in 14 h, whereas the method mentioned in this paper was completed in approximately 8 h. We begin with a detailed description of our migration-stretch compensation algorithm. We then show the effect of migration stretch on AVO and prestack inversion computed from a simple elastic synthetic model. Next, we apply our algorithm to a

prestack migrated data volume acquired over a Barnett Shale reservoir in the Fort Worth Basin, Texas, showing the improvement in resolution of Z_S and ρ over those obtained by inverting the uncorrected data. Finally, we conclude with a summary of the value and limitations of this workflow.

Methodology

NMO and NMO stretch

The traveltime for a flat and homogeneous isotropic layer is hyperbolic. If the vertical two-way traveltime is given by T_0, then the traveltime for the same reflector at source-receiver offset h for velocity v_{rms} is approximated by

$$t(T_0, v_{\text{rms}}, h) = \left\{ T_0^2 + \left[\frac{h}{v_{\text{rms}}(T_0)} \right]^2 \right\}^{1/2}, \tag{1}$$

where each trace is defined by a fixed offset h. The change in two-way traveltime t as a function of the zero-offset traveltime T_0 is

$$\frac{\partial t}{\partial T_0} = T_0 \left\{ T_0^2 + \left[\frac{h}{v_{\text{rms}}(T_0)} \right]^2 \right\}^{-1/2} < 1. \tag{2}$$

Wavelet decomposition

Let us assume that an earth model is composed of a suite of J reflections at time t_j and reflection coefficient r_j. Let's also assume that the time-varying source wavelet can be represented by Morlet wavelets of the form $w(f_j, \phi_j)$, where f_j and ϕ_j are the frequency and phase of the wavelets. The seismic trace without the NMO correction is then

$$u(t^{\text{RNMO}}) = \sum_{j=1}^{J} r_j \delta(t_j^{\text{RNMO}}) w(f_j, \phi_j), \tag{3}$$

where the superscript RNMO indicates that the times are measured after reverse NMO. After a conventional sample-by-sample NMO correction, these wavelets are stretched, which leads to lower frequencies in the far-offset data for noninterfering events.

Compensation for migration stretch

Rather than starting with uncorrected gathers, most interpreters start with prestack time-migrated data volumes. In addition to placing the data in a more appropriate lateral position, prestack migration also reduces the CMP smear. Velocity analysis of smeared CMP gathers over dipping reflectors results in velocities that are erroneously high. Deregowski (1990) recognizes this shortcoming and develops a workflow (called the Deregowski loop) whereby prestack time-migrated gathers are subjected to reverse NMO, from which velocity spectra are computed and analyzed. These new velocities then can be used by NMO to better align the gathers (e.g., Mutlu and Marfurt, 2015) or, in Deregowski's (1990) case, to remigrate the data.

Let us assume that our migration velocities were (1) sufficiently accurate and (2) provided by the service company along with the migrated gathers. Applying reverse NMO followed by NMO using the same velocity reproduces the original migrated data. Zhang et al. (2013) apply reverse NMO and then construct a wavelet decomposition on the reverse-NMO corrected gathers, in which each wavelet (rather than each sample) was subjected to a subsequent NMO correction, thereby eliminating NMO stretch.

Our modification is simple, but it also is quite efficient. Here, we represent each migrated trace using the same method as in equation 3:

$$u(T_0) = \sum_{j=1}^{J} r_j \delta(T_{0j}) w(f_j, \phi_j), \tag{4}$$

where the time axis T_0 indicates that the reflection event times already have been migrated (or NMO corrected). We can compensate for migration stretch by computing a wavelet compression factor c by mapping t_{0j} to t_j, using equation 5:

$$c_j = \frac{1}{T_{0j}} \left\{ T_0^2 + \left[\frac{h}{v_{\text{rms}}(T_0)} \right]^2 \right\}^{1/2} > 1, \tag{5}$$

which can then be used to scale the wavelets in equation 4 and generate the compensated trace:

$$u_{\text{comp}}(T_0) = \sum_{j=1}^{J} r_j \delta(T_{0j}) w(c_j f_j, \phi_j). \tag{6}$$

The input to the algorithms consists of migrated seismic gathers and either a root-mean-square (rms) or migration velocity model (Figure 2). The output is a volume of gathers that have been compensated for migration stretch.

Implementation of matching pursuit in stretch compensation

Matching pursuit (e.g., Castagna and Sun, 2006; Liu and Marfurt, 2007) works in a manner similar to high-resolution Radon transforms, in which the spectra of the strongest events are estimated and subtracted from the trace first, followed by iterative estimation and subtraction of successively weaker events. Since their original introduction, more general basis pursuit algorithms that use a suite of nonorthogonal basis functions as well as L1 norms applied to the data misfit and L1 constraints to minimize the number of components have been found to be quite effective in improving the resolution of seismic data (e.g., Puryear and Castagna, 2008). We provide an updated description of the relatively simple matching pursuit algorithm used by Liu and Marfurt (2007).

We begin the analysis by assuming that each seismic time trace $u(t)$ is band-limited and can be represented by a linear combination of J Morlet wavelets w:

$$u(t) = \sum_{j=1}^{J} r_j \cdot w(t - t_j, f_j, \phi_j) + n(t), \tag{7}$$

where r_j, t_j, f_j, and ϕ_j represent the reflection coefficient, center time, peak frequency, and phase of the jth wavelet centered about time t_j and $u(t)$ represents noise. In general, reflected events from thin beds, gradients in impedance, discontinuities in attenuation (1/Q), and inaccurately migrated events, as well as dispersed events, will have arbitrary phases even if the source wavelet is of zero phase. For this reason, we construct our basis functions using a suite of complex Morlet wavelets (Figure 3). We calculate the center time t_j of each candidate wavelet using the peaks in the instantaneous envelope and the wavelet frequency, f_j, using the instantaneous frequency at the envelope peak.

The temporal behavior of a zero-phase Morlet wavelet is given by

$$w(t, f_j) = \exp(-t^2 f_j^2 \cdot 2 \ln 2) \cdot \cos(2\pi f_j t), \tag{8}$$

whereas its magnitude spectrum is given by

$$\bar{w}(f, f_j) = \frac{\sqrt{\pi / \ln 2}}{f_j} \cdot \exp\left[-\frac{\pi^2 \left(f - f_j\right)^2}{2 \ln 2 \cdot f_j^2}\right] \tag{9}$$

To efficiently solve for the magnitude and phase of each wavelet, we use the Hilbert transform and form an analytic data trace $U(t)$:

$$U(t) = u(t) + iu^H(t), \tag{10}$$

and a table of analytic complex wavelets:

$$W(t, f_j) = w(t, f_j) + iw^H(t, f_j), \tag{11}$$

where w are symmetric cosine wavelets given by equation 8 and w^H are antisymmetric sine wavelets (Figure 3).

The first step in the matching pursuit algorithm is to precompute a finely sampled wavelet dictionary that spans the bandwidth of the input data. The analytic analog of equation 7 then becomes

$$U(t) = \sum_j A_j \cdot W_j(t - t_j, f_j) + N(t), \tag{12}$$

where

$$e(t) = \|U(t)\|, \tag{13}$$

$$A_j = r_j e^{i\phi_j}, \tag{14}$$

and where $e(t)$ is the instantaneous envelope of the seismic trace and r_j and ϕ_j represent the magnitude and phase of the complex wavelet W_j.

Our objective is to minimize the energy of the residual analytic trace $R(t)$ defined as the squared difference between the analytic seismic trace and the matched wavelets:

$$\|R(t)\|^2 = \|U(t) - \sum_j^J [A_j W_j(t - t_j, f_j)]\|^2. \tag{15}$$

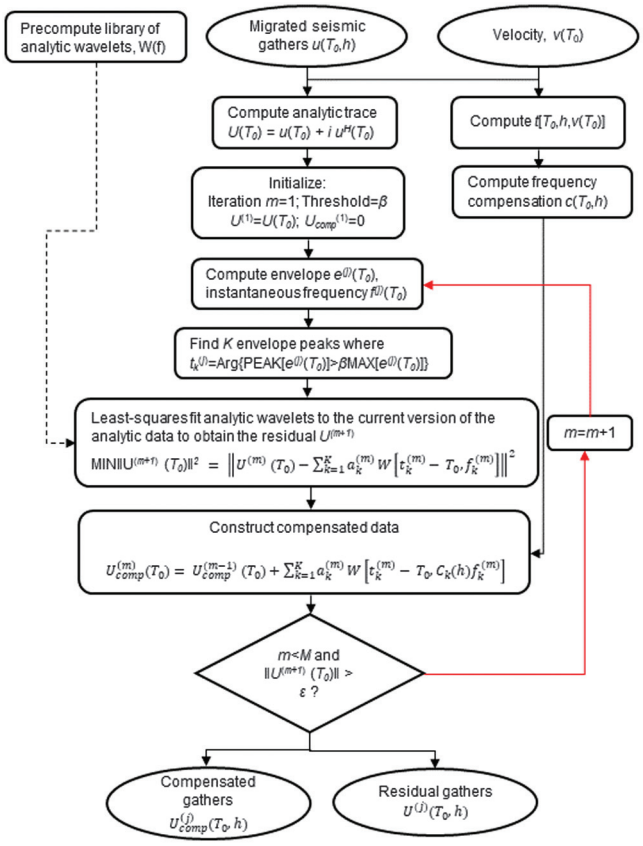

Figure 2. Flowchart of the migration stretch-compensation algorithm. The input to the program is unmuted prestack time-migrated gathers and the velocities used to migrate the data.

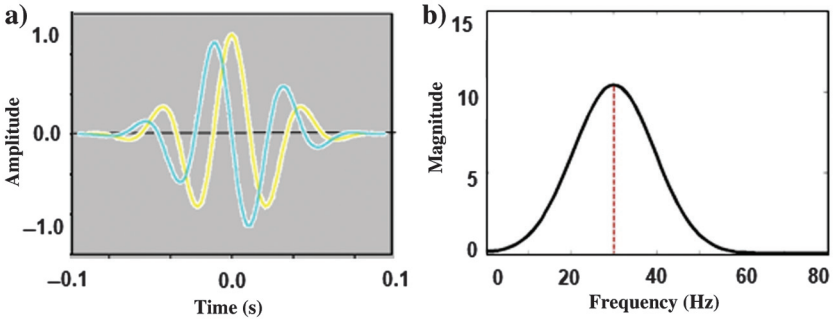

Figure 3. (a) A complex 30 Hz Morlet wavelet consisting of a real part or 0° Morlet wavelet (yellow) and an imaginary part or 90° Morlet wavelet (cyan) and (b) the corresponding magnitude spectrum (after Liu, 2006).

If we were to attempt to estimate all wavelet coefficients in one iteration, we would write equation 15 in matrix form and solve the normal equations:

$$\mathbf{A} = [\mathbf{W}^{\mathbf{H}}\mathbf{W} + \varepsilon\mathbf{I}]^{-1}\mathbf{W}^{\mathbf{H}}\mathbf{U}, \qquad (16)$$

where $\mathbf{W} = [W(t,f_1), W(t,f_2), \ldots, W(t,f_m)]$ is a vector of wavelets centered of known frequency at each known envelope peak; $\mathbf{A} = (A_1, A_2, \ldots A_m)$ is a vector of unknown complex wavelet amplitudes; $\mathbf{I}$ is the identity matrix; and ε is a small number that makes the solution stable. For seismic data, $\mathbf{A}$ will be a complex-symmetric banded matrix, with the bandwidth proportional to the number of samples used to define the lowest frequency wavelet used and therefore amenable to an efficient solution. Liu's (2006) provides a graphical image of equation 15, where the black and red curves represent the real and imaginary parts of the complex trace and complex wavelets (Figure 4).

Even if we attempted to approximate the seismic data using wavelets centered about all the peaks of $e(t)$, the resulting residual $R(t)$ still may contain weaker seismic events of interest, implying an iterative solution to find them. Alternatively, isolated low-amplitude events may represent noise, implying that we may wish to start with the highest amplitude event, estimate and subtract it, and iteratively repeat the process on the residual, giving rise to what is called a greedy matching pursuit algorithm (Mallat and Zhang, 1993). If we consider a thin bed tuning model in which the top and bottom reflection events are nearly equal, resolvable, but interfere with each other, it is clear that the greedy matching pursuit will be biased. For this reason, Liu and Marfurt (2007) provide a parameter $0 \le \beta \le 1$ that allows the interpreter to adjust how many events $k = 1, 2, \ldots, K$ of the J envelope peaks are used in each iteration. Specifically,

$$k = \begin{cases} j & \text{if } e_k \ge \beta \underset{j}{\text{MAX}}(e_j) \\ \text{null} & \text{if } e_k < \beta \underset{j}{\text{MAX}}(e_j) \end{cases}, \qquad (17)$$

where "null" indicates that that event is not used. The iteration continues until either an acceptable residual has been reached or the convergence rate slows down to a level indicating numerical convergence.

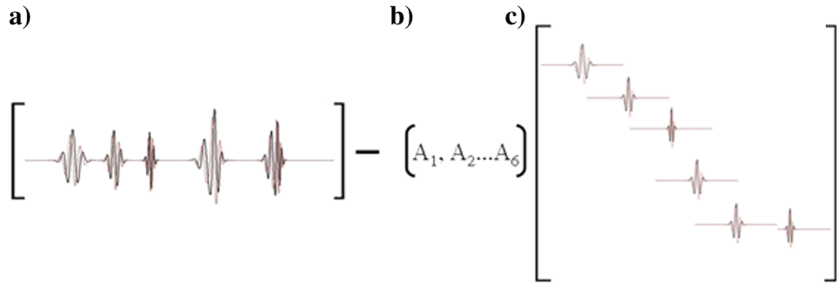

Figure 4. (a) A complex seismic trace represented by (b) six complex amplitudes and (c) six complex Morlet wavelets. The goal of equation 15 is to compute the complex wavelet amplitudes *Aj* that, when multiplied by *Wj* and summed, approximate the complex seismic trace in a least-squares sense (after Liu, 2006).

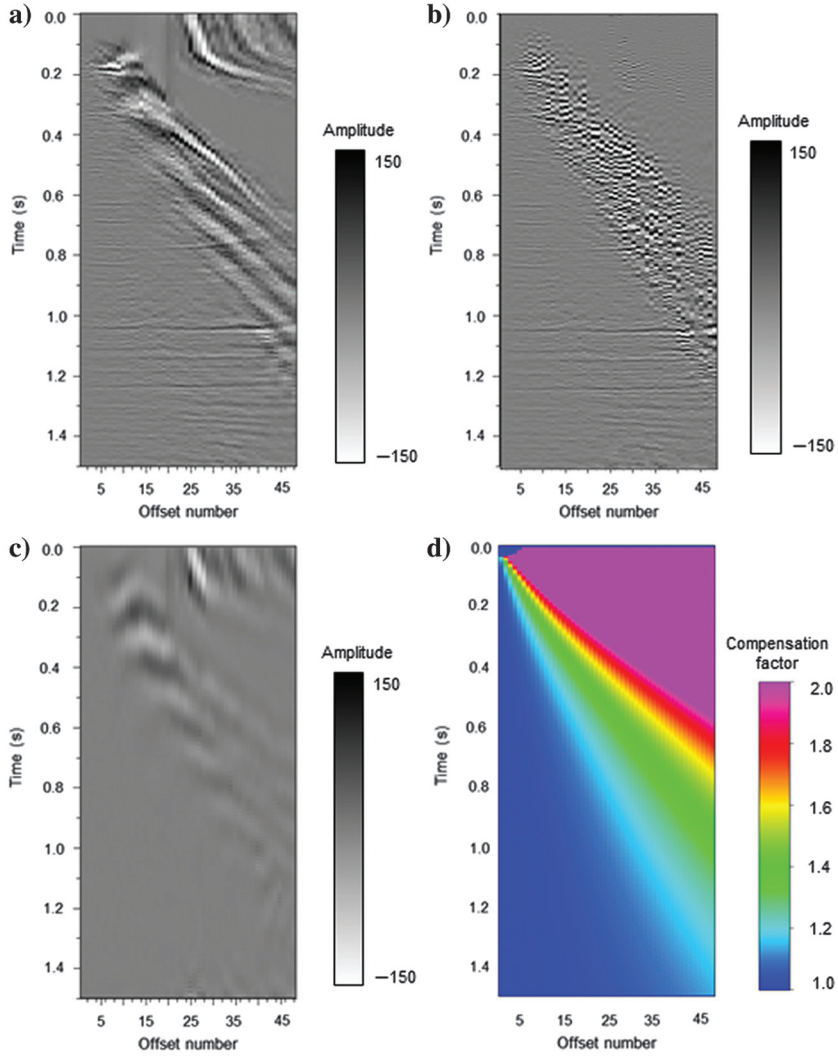

Figure 5. (a) The unmuted CRP gather of the data, (b) unmuted migration stretch-compensated CRP gather, (c) unmodeled data, and (d) the frequency compensation factor. The compensation factor increases with increasing offset and decreases with increasing time.

To compensate for migration stretch, we replace the wavelets given by equation 7 with the "nonstretched" wavelets f_k with compensated wavelets $c_k f_k$ described by equations 5 and 6. We also apply the phase shift occurring in A_j to the real wavelet w rather than to the reflection coefficient r_j:

$$
\begin{aligned}
u(t) &= \mathrm{Re}[U(t)] \\
&= \mathrm{Re}\left[\sum_{j=1}^{J} r_j \exp(i\varphi_j) W_j(t - t_j, f_j) + N(t)\right] \\
&= \sum_{j=1}^{J} r_j w_j(t - t_j, f_j, \varphi_j) + n(t). \qquad (18)
\end{aligned}
$$

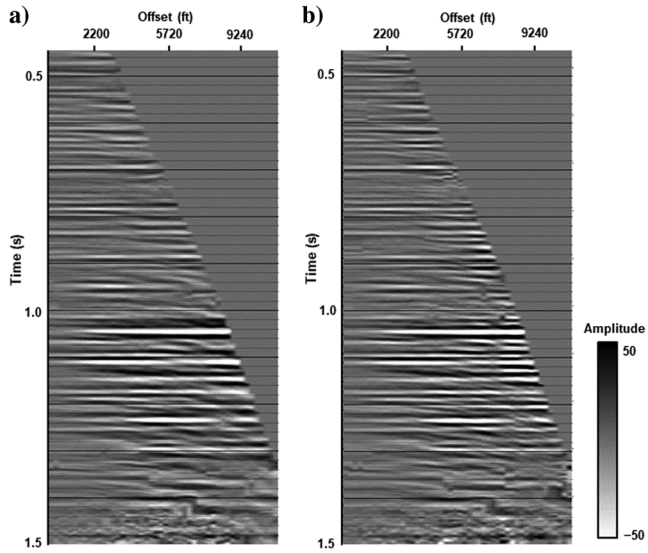

Figure 6. The (a) original migrated and (b) stretch-compensated CRP gathers corresponding to Figure 3a and 3b, but now after data conditioning. The same suite of conditioning steps and parameters has been applied to both data volumes. Note how stretch compensation increased the resolution of the long-offset data, leaving the near offset unchanged.

Application

Results after compensating for migration stretch

We apply the algorithm to a wide-azimuth seismic survey acquired over the Fort Worth Basin. The depth of the Barnett Shale target is approximately 5600 ft, whereas the offset of farthest migrated gather is 10,560 ft. The sweep of the vibrator was 120 Hz. The data were prestack time-migrated using a Kirchhoff algorithm. Figure 5a shows an unmuted common reflection point (CRP) gather from the data. Figure 5b shows the migration stretch compensated

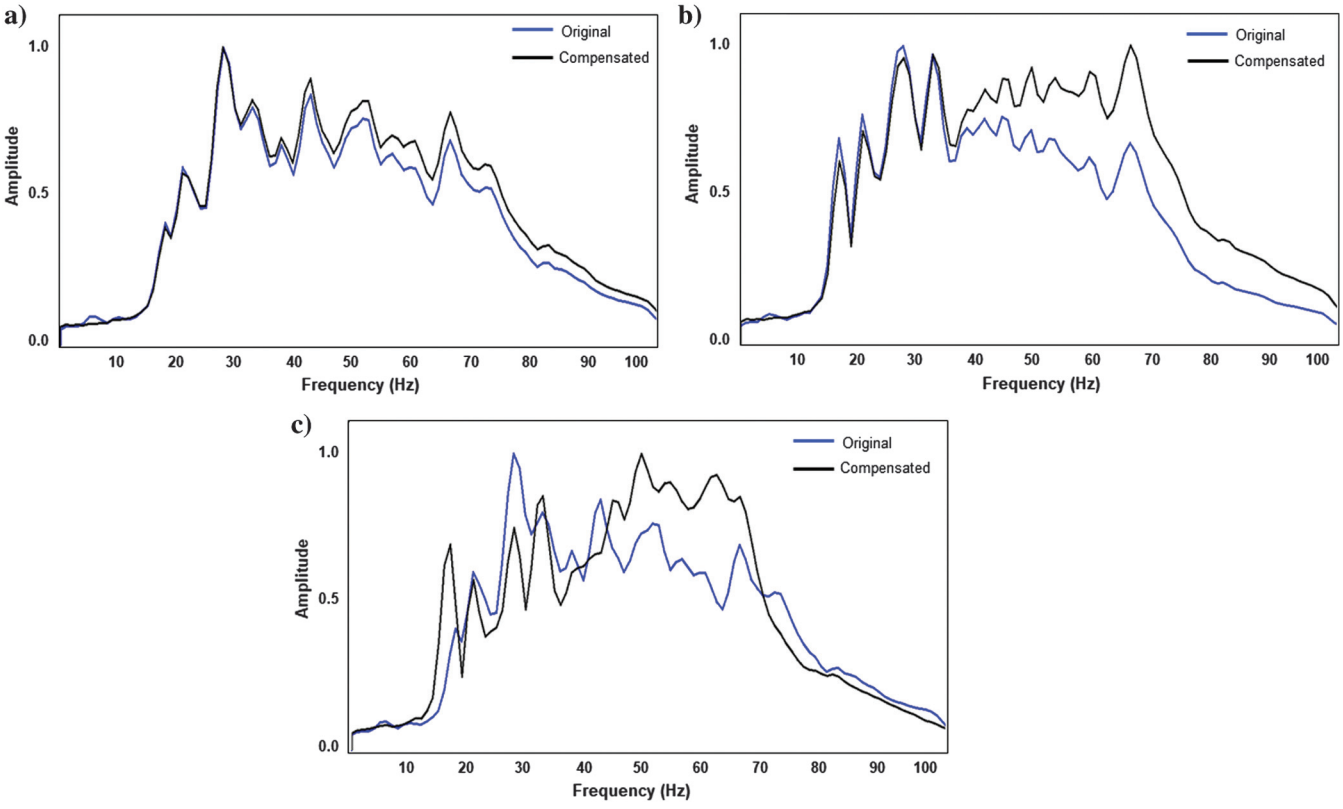

Figure 7. Amplitude spectrum of the original and the compensated gathers for (a) near-angle CRP gather (6°–20°), (b) mid-angle CRP gather (20°–34°), and (c) far-angle CRP gather (34°–42°). Compensation for the migration stretch increases the ratio of high frequency to the overall spectrum.

DOI:10.1190/INT-2019-0226.1

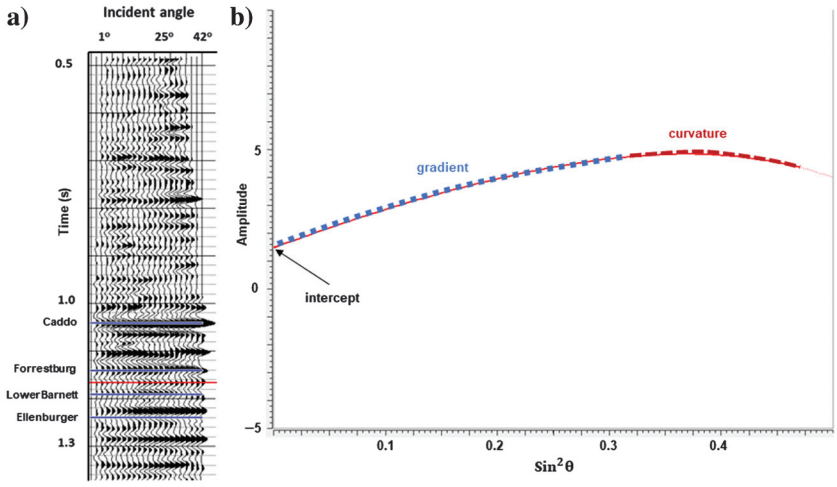

Figure 8. (a) The angle gathers corresponding to the compensated gather shown in Figure 4b with reflectors of interest highlighted in blue and (b) the AVO response of the event indicated by the red line in (a). The blue dashed line indicates the approximate AVO gradient. The red dashed line indicates the AVO curvature.

unmuted CRP gather. Figure 5c shows the data not modeled by the matching pursuit algorithm. The unmodeled is the uncompensated data. The algorithm compensates for significantly greater amounts of stretch mute, where the default value of 100% will compress correspondingly stretched wavelets by a factor of 2. The unmodeled data is the one stretched above 100%. Figure 5d shows the frequency compensation factor. The compensation factor increases with offset and decreases with depth, such that the far-offset data of the shallower zone suffer from more significant stretching. Figure 5b shows an increase in resolution at the farther offsets at the Barnett Shale target at t = 1.1 s when corrected for migration stretch.

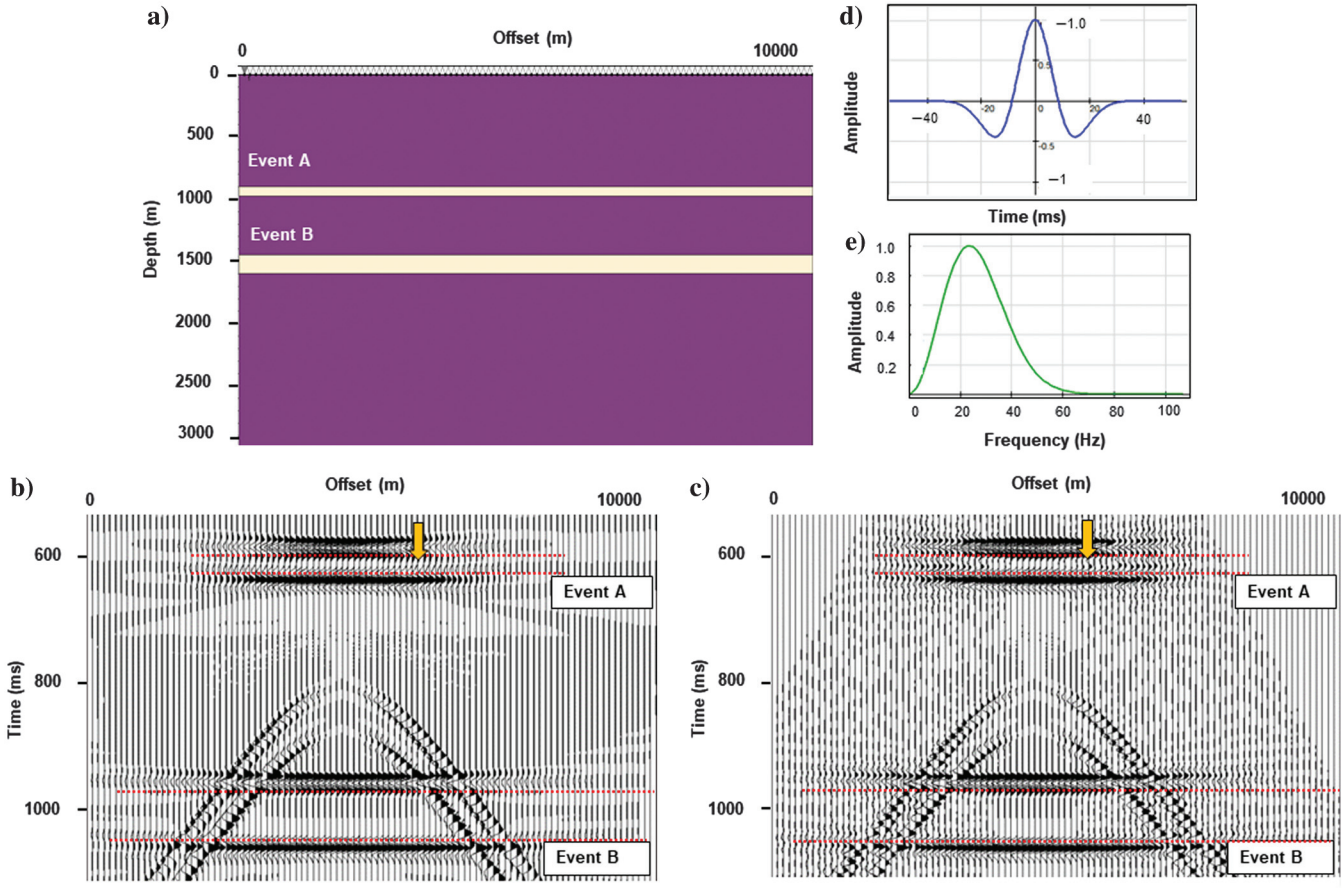

Figure 9. (a) A simple model constructed to show the change of tuning with offset. Layer A is 50 m thick, whereas layer B is 150 m thick. The thickness of event A is just more a quarter wavelength of the source wavelet. The Z_P of both events is 7200 (m/s * g/cm^3), whereas the Z_P of the background model is 6900 (m/s * g/cm^3). (b) PSTM CMP gather of the 2D elastic modeling response of the model. The yellow arrow indicates the offset where it is challenging to resolve event A due to stretching of the top and bottom reflectors of the event. (c) Migration stretch-compensated CMP gather of the 2D elastic modeling response of the model. The yellow arrow indicates artifacts caused due to incorrect representation of the composite wavelet for the event. The source wavelet (Ricker) in the (d) time domain and (e) frequency domain. The red dashed lines show the top and bottom of the events. The modeling shows a decrease in the resolution of event A with offset (the yellow arrows). The elastic modeling also shows interference of positive (the top of event A) and negative (the bottom of event A) amplitudes at the far offset, leading to the thickness of event A being unresolved at the far offset.

Data conditioning

Migrated gathers often are contaminated by noise, and they may require a residual moveout or even muting prior to AVO or prestack inversion analysis. To ascertain changes caused by migration stretch compensation, the same suite of conditioning steps and parameters were applied to both volumes. First, we applied a seismic mute to remove high-amplitude reverberations that overprint the shallow far-offset data. Then we applied a parabolic Radon transform to discriminate between primaries and long period multiples. Next, we suppress the noise crosscutting the reflectors of interest by applying prestack structure-oriented filtering (Zhang et al., 2016; Sinha et al., 2017) using a lower upper median filter. Finally, we apply trim statics to better align the reflectors horizontally. Figure 6a and 6b shows the same gathers shown in Figure 5 after data conditioning. Compensating for migration stretch has considerably improved the resolution of the far-offset data. Figure 7 compares the amplitude spectra of original and compensated near-, mid-, and far-angle traces. Figure 7a shows that stretch compensation has a limited effect on the amplitude spectrum of near incident angles. Examining the compensation factor in Figure 5d shows only a small factor C for near incident angles that increases as the incident angle increases, which is validated by the increase in high frequencies for the mid- and far-angle traces (Figure 7b and 7c).

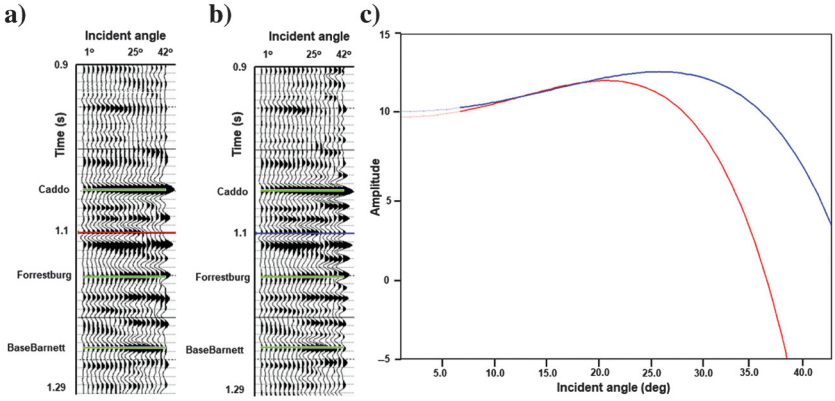

Figure 10. The angle gather of (a) original and (b) compensated prestack data with the reflectors of interest highlighted by green lines. (c) The red and blue line shows the AVO curve for original and compensated gather for an event at 1.1 s highlighted by the red and blue line in (a) and (b) respectively. The AVO curve has been derived using Aki and Richards' three-term approximation equation.

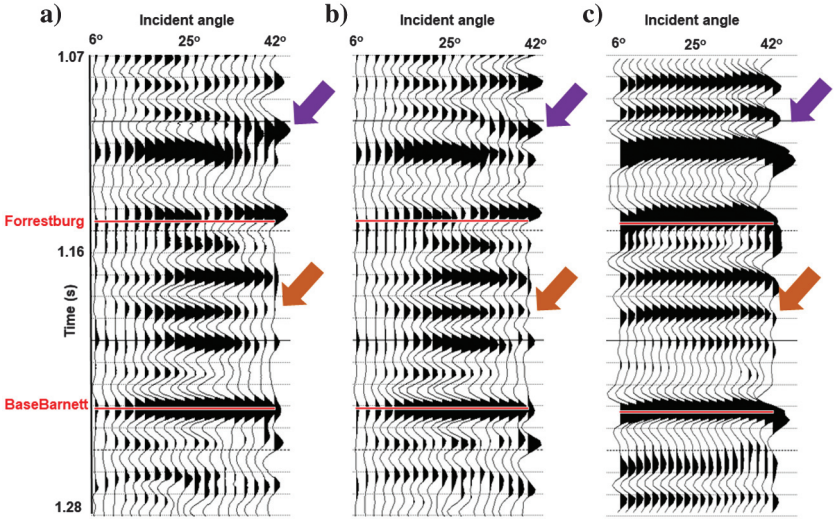

Figure 11. (a) The original, (b) stretch-compensated, and (c) forward-modeled angle gather. The purple arrow in (a) shows the far-offset gather where two events intersect each other due to stretching but are resolved after stretch compensation in (b) as shown by the forward-modeled gather in (c). The orange arrow indicates an event in which a decrease in amplitude is observed in the original gather, unlike the modeled gather, but stretch compensation restores the amplitude at the far offset.

Effect of stretching on AVO

Zoeppritz's (1919) equations describe the partitioning of the P- and S-wave energy into transmitted and reflected components as a function of incident angle. Figure 1 shows a cartoon of conventional PP seismic data acquisition. For flat-layered geology and vertical incidence, almost 100% of the near-offset reflected energy consists of PP reflections. At farther offsets, the P-wave energy is converted to PP and PS reflections and transmissions, which leads to the PP reflection at far offsets being sensitive to Z_S and ρ. Unless we acquire multicomponent data, we do not directly measure the PS reflection events. Rather, it is the sensitivity of the PP reflection events to the incident angle that allows us to invert for Z_S and ρ. The three-term approximation of Zoeppritz's equations developed by Aki and Richard (1980) shows that Z_P, Z_S, and ρ can be estimated from the coefficients (intercept, gradient, and curvature) of the three-term approximation equations, which are calculated from PP reflected waves as a function of incident angles (Figure 8). The intercept is the zero-angle reflection coefficient, which is related to the acoustic impedance contrast across the reflector. The gradient is related to the shear and acoustic impedance contrast across the interface. The third coefficient (curvature), which measures the curvature of the amplitude near the critical angle, is greatly influenced by the density contrast across the interface. Because the offset is small, the recorded seismic wavefield does not suffer from migration stretch. At farther offsets (Figure 1b), the PP-reflected

event now suffers from migration stretch. Because the farther offset is sensitive to Z_S and ρ, the lower resolution of Z_S and ρ compared to that of Z_P is partially attributed to migration stretch.

Inversion results for reflectors that fall near the tuning frequency are particularly affected by migration stretch, which we demonstrate using the elastic finite-difference model shown in Figure 9. Figure 9a shows a sketch of the model used for modeling the migration stretch effect on tuning beds. The Z_P value of the background model is 6900 ($m/s \times g/cm^3$). The Z_P value of the top and bottom events is 7200 ($m/s \times g/cm^3$), but they are 50 and 150 m thick, respectively. The acquisition consists of 100 receivers and 100 sources spread across a 10,000 m offset. The elastic wave propagation was carried out using a Ricker wavelet of 25 Hz peak frequency. The CMP gather was then prestack time migrated (PSTM) to obtain Figure 9b. The stretching causes interference of positive and negative amplitude responses of the top and bottom of event A, which in turn causes the resolution loss of event A with offset, which is just above the tuning resolution, disappearing at the farthest offset. Figure 9c shows that the applied migration stretch compensation algorithm provides good, but not perfect, improvement to the thin, tuned event A by broadening the spectrum. The algorithm introduces positive and negative amplitudes at the offset where it was supposed to compensate for stretch to resolve event A. This is because the composite amplitude of those spectral components that fall below thin-bed tuning is incorrectly represented by a composite wavelet with a 90° phase change. The compensation algorithm then inaccurately represents this part of the spectrum by a broader band but 90° phase wavelet that falls in the middle of the thin bed. Event B is less affected by stretching because it is significantly thicker than the tuning resolution. The composite amplitude for the better components of the amplitude spectrum is accurately corrected, like the event at 1.1 s in Figure 10a and 10b that are adequately resolved, giving rise to higher positive and negative amplitudes at the farther offsets that previously suffered from destructive interference.

The events in Figure 10a and 10b show improvement in resolution at far offset after compensating for migration stretch. The reflectors, which gradually disappear at far offsets due to the interference of over- and underlying reflectors caused by stretching, appear stronger after the compensation (the reflector highlighted by the red and blue lines in Figure 10). Figure 10 shows that such interference causes false amplitude signatures at far offset for the reflector bounded by the interfering reflectors, which in turn leads to an inaccurate AVO signature. The positive-amplitude event at 1.1 s (Figure 10) shows a phase reversal at the far offset in the original angle gather. In reality, the phase reversal is caused by interference of negative-amplitude reflectors over- and underlying this positive-amplitude event. The compensation causes resolution balancing over the entire reflector, which leads to the appearance of the positive amplitudes at far offset, which was hidden by stretching and interference. We confirm the fidelity of the appearance of amplitude at far offsets by comparing the original and compensated gathers with the forward-modeled angle gather (Figure 11). Unlike the modeled angle gather (the purple arrow in Figure 11c), the negative-amplitude reflector at 1.1 s disappears at the far offset due to stretching and interference of overlying and underlying positive-amplitude reflectors (the purple arrows in Figure 11a). The stretch compensation algorithm improves the resolution of far-offset data leading to the appearance of a negative-amplitude reflector at the far offset as shown by the modeled angle gather data (the purple arrow in Figure 11b). Due to balanced resolution, the events appear continuous after stretch compensation as predicted by the modeled data (Figure 11c). The stretch compensation also improves the amplitude consistency across the offset as predicted by the modeled gather (the events shown by the orange arrow in Figure 11).

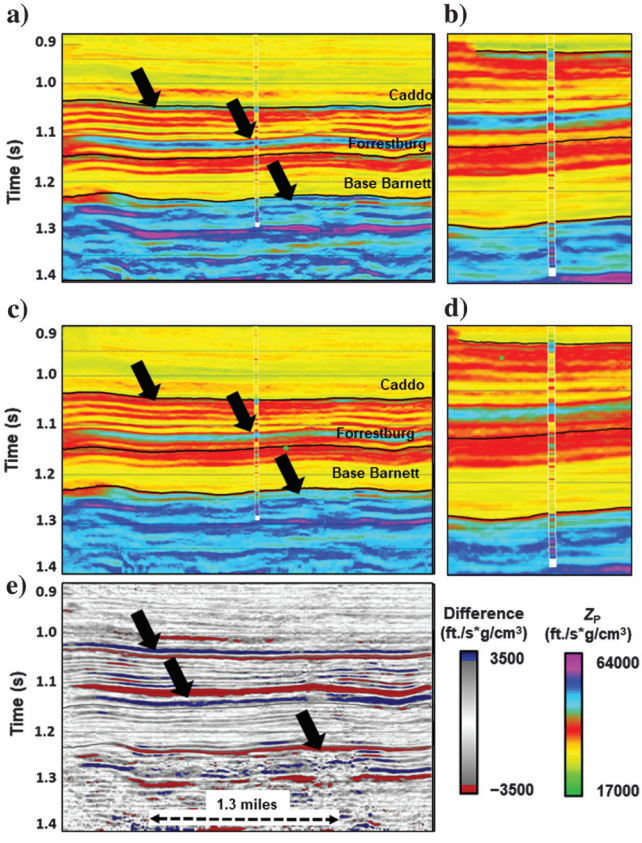

Figure 12. The term Z_P estimated from simultaneous inversion of the (a) original prestack and (c) migration stretch-compensated prestack gathers and (e) the difference between (b) and (a) (compensated-original). (b and d) Close-up view near the well of (a) and (b), respectively, showing a change in Z_P with respect to the well after stretch compensation. The black arrows indicate areas where significant changes in Z_P are observed. An insignificant change is observed in the resolution after compensation.

Prestack simultaneous inversion

Simultaneous inversion to estimate Z_P, Z_S, and ρ are critical in many resource plays. The terms Z_P and Z_S can be correlated to mineralogy and hence brittleness using ECS or other mineralogy logs, which in turn can map areas that are amenable to hydraulic fracturing. Volumetric estimates of ρ can be correlated to log measurements and core analysis to predict areas that have total organic carbon. The maximum usable incident angle of 42° at the Barnett Shale target allowed us to estimate ρ from inversion. Angles beyond 42° were contaminated by strong linear noise from the shallow section; they also fall beyond the critical angle and are not useful for inversion. The inversion of both data volumes was carried out with the same parameters. Figure 11a and 11c shows the Z_P estimated from simultaneous inversion of the original prestack-migrated and migration stretch-compensated gathers, respectively. A good match between the $Z_P{}^{log}$ and $Z_P{}^{seismic}$ (impedances measured by well logs and seismic inversion) confirms the fidelity of the inversion (Figure 12b and 12d). Compared with well Z_P, we do not see significant improvement in Z_P after stretch compensation.

The difference between $Z_P{}^{original}$ and $Z_P{}^{compensated}$ (Figure 12e) highlights the area of significant change. The maximum change in Z_P occurs near the fast rocks (limestone and basement). During prestack inversion, Z_P is not independently estimated from zero-offset traces; rather, it is calculated from the coefficients of the three-term linear approximation equation. Stretch compensation causes a change in the values of those coefficients by changing the AVO response. The AVO is a function of impedance contrast across the reflector. If the contrast is high, the change in AVO before and after compensation will be high (Figure 13). Hence, we observe a maximum change in Z_P near the fast rocks (Caddo, Forrestburg, Ellenberger, and Basement). The change observed in Figure 12e is attributed to change in the AVO response. There is an insignificant change in Z_P after stretch compensation away from the fast rocks.

Figure 14a and 14c shows Z_S from prestack simultaneous inversion for the original and the compensated gathers. The black arrows in Figure 14e highlight the areas of maximum change. These changes can be attributed to a change in the AVO response and an increase in resolution. The gray arrows indicate areas where an increase in resolution is observed. A significant increase in resolution is obtained in the shallower zone than in the deeper because the wavelet compensation factor applied in the methodology decreases with depth and increases with angle of incidence (Figure 5c). Figure 14b and 14d shows the change in Z_S near the well. A good match between the well and seismic shows the fidelity of the inversion. We do see a significant change in resolution near the well and far away from the well; some of them are highlighted by the gray arrows in Figure 14c.

A maximum usable incident angle of 42° at the Barnett Shale allowed us to invert the prestack data for density during simultaneous prestack inversion. The ρ results for the original and compensated gathers are

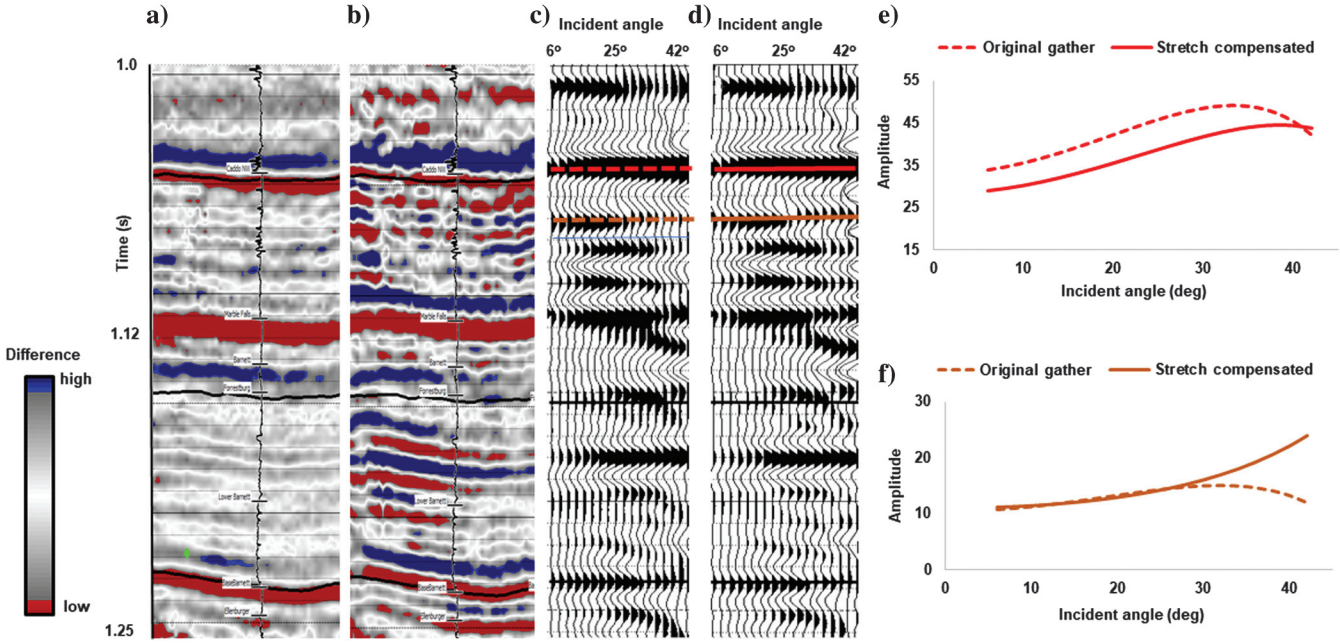

Figure 13. The difference between the original and the stretch-compensated (a) Z_P (compensated-original), (b) ρ (compensated-original). Angle gathers: (c) original and (d) stretch-compensated. (e) AVO curve of the Caddo Formation shown by the red line in (c) and (d). (f) AVO curve of the formation shown by the orange line in (c) and (d). We can observe that a significant change in AVO occurs near the fast rocks. Hence, we see a change in Z_P near the fast rocks. Whereas away from the fast rocks, we do not see a significant change in AVO except the change in curvature above 35° (the orange curve in [f]), which is reflected by an insignificant change in Z_P and a considerable change in ρ.

shown in Figure 15a and 15c, respectively. The black arrows in the difference volume (Figure 15e) indicate areas near the fast reflectors, where the maximum change in ρ is observed. We attribute these changes to a change in AVO response and an increase in resolution. The gray arrows indicate areas away from the faster reflectors where the change in density is attributed to the increase in resolution. Compared with the density logs, Figure 15b and 15d shows that we observe an overall increase in density resolution. As with the Z_S images, the improvement in resolution is higher for the shallower zone than the deeper zone because the compensation factor is higher for the shallower zone.

Limitations

The stretch-compensation we use assumes that the stretch from prestack time migration is approximately the same as caused due to NMO. We believe this to be an accurate approximation for most resource plays in North America, such as the Barnett Shale, which exhibits dips no greater than 2°. Furthermore, commercial prestack impedance inversion software used by oil company quantitative interpreters often assumes the dip of the reservoir to be relatively gentle. The migration stretch compensation algorithm described here (and most commercial inversion software) will not work on steeply dipping reservoirs located on salt flanks and other tectonically complex terrains. These data often require prestack depth migration to be imaged appropriately and will require the development of a stretch-compensation algorithm based on the kinematics of residual moveout algorithms currently in use. Stretch compensation applied on the 2D elastic response of the model suggests that resolution improvement using bandwidth extension methods based on the location of energy peaks such as matching pursuit (Mallat and Zhong (1992), Matos and Marfurt (2014)) cannot extend the resolution of poorly resolved spectral

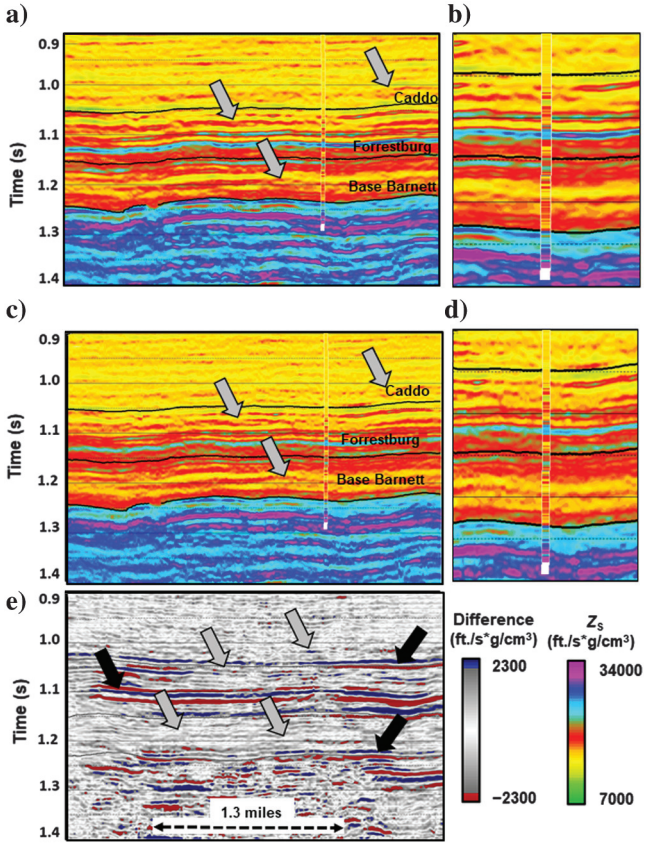

Figure 14. The term Z_S estimated from simultaneous inversion of the (a) original prestack gather and (c) migration stretch-compensated prestack gather and (e) the difference between (b) and (a) (compensated-original). (b and d) Close-up view near the well of (a) and (b), respectively, showing a change in Z_S with respect to the well after stretch compensation. The gray arrows show some of the areas of a significant improvement in the resolution of Z_S from the compensation of the migration stretch. The black arrows point to the zone where the change in Z_S is observed across the whole reflector. These changes might be due to the change in AVO and/or the change in resolution.

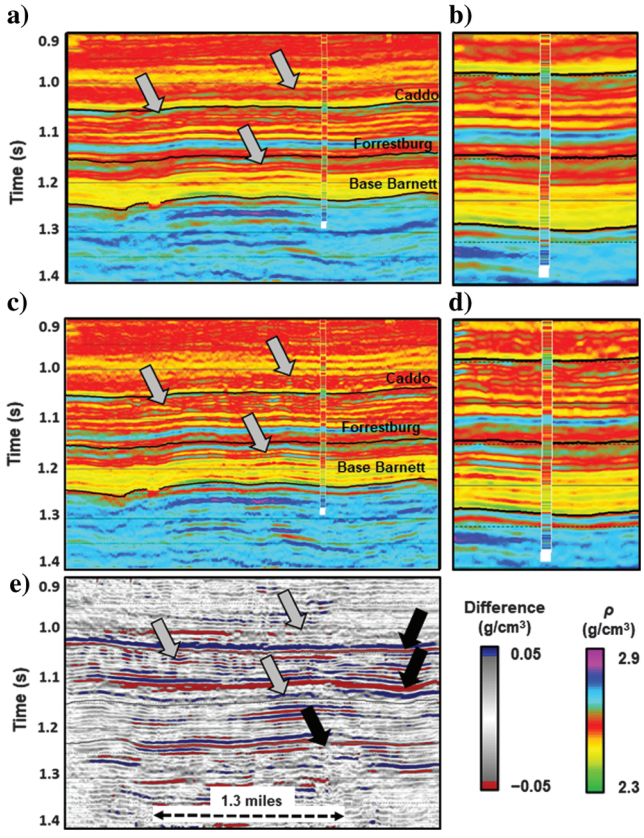

Figure 15. The term ρ estimated from simultaneous inversion of the (a) original prestack gather and (c) migration stretch-compensated prestack gather and (e) the difference between (b) and (a) (compensated-original). (b and d) Close-up view near the well of (a) and (b), respectively, showing a change in ρ with respect to the well after stretch compensation. The gray arrows indicate some of the areas of significant improvement in resolution of ρ by compensating for the migration stretch. The black arrows point to the zone where the change in Z_S is observed across the whole reflector. These changes might be due to the change in AVO and/or the change in resolution.

DOI:10.1190/INT-2019-0226.1

components. The method incorrectly compensates the composite response of the tuned beds at far offsets by a broader band but a 90° phase wavelet that falls in the middle of the bed. This introduces false-positive and negative amplitudes at the offsets, when an increase in bed resolution is expected. A potential solution to this approach is a double-spike inversion approach such as the one described by Puryear and Castagna (2008).

Conclusion

In principle, seismic reflections are represented by discrete spikes at reflector boundaries. These spikes then are convolved with the seismic wavelet to provide the seismic trace. Migration assumes that each sample of the seismic trace is a potential reflection spike, leading to stretch of the imaged wavelets, which in turn leads to a lower resolution for inverted S-impedance and density. Such stretching may give rise to an apparent phase reversal of the reflectors due to interference of the stretched reflectors bounding it, leading to false AVO signatures and inversion results. We use a matching pursuit algorithm to estimate the location of the reflection's spikes, fit wavelets to the data, and then compensate for migration stretch. Comparison of the amplitude spectrum for near-, mid-, and far-angle stacks of the original gather and stretch-compensated gathers shows an increase in higher frequencies. Because the P-impedance is heavily dependent on the zero-angle reflected PP-waves, there is an insignificant improvement in the P-impedance resolution. In contrast, there is a significant improvement in resolution for Z_S and ρ in the shallow section and a moderate improvement in the deeper section. The method shows significant improvement for well-resolved beds, but it incorrectly estimates the composite response of tuned beds at the far offset, leading to the addition of false amplitudes.

Acknowledgments

We thank the Pioneer Natural Resources Company for providing a license to its seismic data for use in research and education. Thanks go to CGG GeoSoftware for the licenses to its Geoview inversion package. The finite-difference synthetic seismic gathers and migrated results were computed using Tesseral Pro. Finally, our thanks go to the sponsors of the AASPI consortium for their guidance and financial support.

Data and materials availability

Data associated with this research are confidential and cannot be released.

References

Abedi, M. M., and M. A. Riahi, 2016, Nonhyperbolic stretch-free normal moveout correction: Geophysics, **81**, no. 6, U87–U95, doi: 10.1190/geo2016-0078.1.

Abedi, M. M., M. A. Riahi, and A. Stovas, 2019, Three-parameter normal moveout correction in layered anisotropic media: A stretch-free approach: Geophysics, **84**, no. 3, C129–C142, doi: 10.1190/geo2017-0855.1.

Aki, K. L., and P. G. Richard, 1980, Quantitative seismology: W. H. Freeman and Co.

Brouwer, J. H., 2002, Improved NMO correction with a specific application to shallow seismic data: Geophysical Prospecting, **50**, 225–237, doi: 10.1046/j.1365-2478.2002.00310.x.

Buchholtz, H., 1972, A note on signal distortion due to dynamic (NMO) corrections: Geophysical Prospecting, **20**, 395–402, doi: 10.1111/j.1365-2478.1972.tb00642.x.

Castagna, J. P., and S. Sun, 2006, Comparison of spectral decomposition methods: First Break, **24**, no. 3, doi: 10.3997/1365-2397.24.1093.26885.

Chen, S., S. Jin, L. Xian-Yang, and W. Yang, 2018, Non-stretching normal-moveout correction using a dynamic time warping algorithm: Geophysics, **83**, no. 1, V27–V37, doi: 10.1190/geo2016-0673.1.

Deregowski, S. M., 1990, Common-offset migrations and velocity analysis: First Break, **8**, 224–234, doi: 10.3997/1365-2397.1990011.

Faccipieri, J. H., T. A. Coimbra, and R. Bloot, 2019, Stretch-free generalized normal moveout correction: Geophysical Prospecting, **67**, 52–68, doi: 10.1111/1365-2478.12702.

Fomel, S, 2007, Velocity-independent time-domain seismic imaging using event slopes: Geophysics, **72**, no. 3, S139–S147, doi: 10.1190/1.2714047.

Hicks, G. J., 2001, Removing NMO stretch using the Radon and Fourier- Radon transforms: 63rd Annual International Conference and Exhibition, EAGE, Extended Abstracts, A-18, doi: 10.3997/2214-4609-pdb.15.A-18.

Hilterman, F., and C. Van Schuyver, 2003, Seismic wide-angle processing to avoid NMO stretch: 73rd Annual International Meeting, SEG, Expanded Abstracts, 215–218, doi: 10.1190/1.1817768

Liu, J., 2006, Spectral decomposition and its application in mapping stratigraphy and hydrocarbons: Ph.D. dissertation, University of Houston.

Liu, J., and K. J. Marfurt, 2007, Instantaneous spectral attributes to detect channels: Geophysics, **72**, no. 2, P23–P31, doi: 10.1190/1.2428268.

Mallat, S., and Z. Zhang, 1993, Matching pursuit with time-frequency dictionaries: IEEE Transactions in Signal Processing, **41**, 3397–3415, doi: 10.1109/78.258082.

Mallat, S., and S. Zhong, 1992, Characterization of signals from multiscale edges: IEEE Transactions on Pattern Analysis and Machine Intelligence, **14**, 710–732, doi: 10.1109/34.142909.

Masoomzadeh, H., P. J. Barton, and S. C. Singh, 2010, Nonstretch moveout correction of long offset multichannel seismic data for subbasalt imaging: Example from the North Atlantic: Geophysics, **75**, no. 4, R83–R91, doi: 10.1190/1.3443579.

Matos, M., and K. J. Marfurt, 2014, Complex wavelet transform spectral broadening: 84th Annual International Meeting, SEG, Expanded Abstracts, 1465–1469, doi: 10.1190/segam2014-1369.1.

Mutlu, O., and K. J. Marfurt, 2015, Improving seismic resolution of prestack time-migrated data: Interpretation, **3**, no. 4, T245–T255, doi: 10.1190/INT-2014-0260.1.
Perroud, H., and M. Tygel, 2004, Nonstretch NMO: Geophysics, **69**, 599–607, doi: 10.1190/1.1707080.
Puryear, C., and J. P. Castagna, 2008, Layer-thickness determination and stratigraphic interpretation using spectral inversion: Theory and application: Geophysics, **73**, no. 2, R37-R48, doi: 10.1190/1.2838274.
Rupert, G. B., and J. H. Chun, 1975, The block move sum normal moveout correction: Geophysics, **40**, 17–24, doi: 10.1190/1.1440511.
Shatilo, A., and F. Aminzadeh, 2000, Constant normal-moveout (CNMO) correction: A technique and test results: Geophysical Prospecting, **48**, 473–488, doi: 10.1046/j.1365-2478.2000.00190.x.
Sinha, S., K. J. Marfurt, D. Devegowda, R. Pires de Lima, and S. Verma, 2017, Seismic inversion based SRV and reserves estimation for shale plays: SPE Annual Technical Conference and Exhibition, SPE-187137-MS.
Taner, M. T., and F. Koehler, 1969, Velocity spectra-digital computer derivation applications of velocity functions: Geophysics, **34**, 859–881, doi: 10.1190/1.1440058.
Trickett, S., 2003, Stretch-free stacking: 73rd Annual International Meeting, SEG, Expanded Abstracts, 2008–2011, doi: 10.1190/1.1817723.
Zhang, B., T. Lin, S. Guo, O. E. Davogustto, and K. J. Marfurt, 2016, Noise suppression of time-migrated gathers using prestack structure-oriented filtering: Interpretation, **4**, no. 2, SG19–SG29, doi: 10.1190/INT-2015-0146.1.
Zhang, B., K. Zhang, S. Guo, and K. J. Marfurt, 2013, Non-stretching NMO correction of prestack time-migrated gathers using a matching-pursuit algorithm: Geophysics, **78**, no. 1, U9–U18, doi: 10.1190/geo2011-0509.1.
Zoeppritz, K., 1919, Uber Erdbebenwellen VII b: Gottinger Nachrichten, 66–84.

Swetal Patel received his M.S. (2015) in petroleum engineering and a Ph.D. (2020) in geophysics from the University of Oklahoma under the supervision of K. Marfurt. He has worked as a research assistant in the Integrated Core Characterization Laboratory (IC^3) for three years, conducting experiments on hydraulic fracturing and acoustic emissions to understand the effect of fatigue on fracture growth and propagation. His research interests include AVO, 4D seismic, seismic data conditioning, reservoir characterization by integrating rock physics, and machine learning.

Francis Oyebanji received an M.Sc. (2019) in geophysics from the University of Oklahoma. His thesis work involved fracture characterization of unconventional Woodford Shales resources. He worked as a research assistant for the Institute of Reservoir Characterization (IRC) consortium as a database specialist and the Attribute Assisted Seismic Processing and Interpretation (AASPI) consortium. He is a member of SEG and AAPG. He is currently working for AASPI and pursuing a graduate program in data science and analytics with interest in geostatistics and application of modern machine-learning techniques in improving seismic interpretation.

Kurt J. Marfurt received a Ph.D. (1978) in applied geophysics from Columbia University's Henry Krumb School of Mines in New York, where he also taught as an assistant professor for four years. He joined the University of Oklahoma in 2007, where he serves as the Frank and Henrietta Schultz professor of geophysics within the ConocoPhillips School of Geology and Geophysics. He worked for 18 years in a wide range of research projects at Amoco's Tulsa Research Center, after which he joined the University of Houston for eight years as a professor of geophysics and as the director of the Allied Geophysics Lab. He has received the following recognitions: SEG best paper (for coherence), SEG best presentation (for seismic modeling), as a coauthor with S. Chopra for best SEG poster (for curvature) and best AAPG technical presentation, and as a coauthor with R. Perez-Altamar for best paper in *Interpretation* (on a resource play case study). He also served as the SEG/EAGE Distinguished Short Course Instructor for 2006 (on seismic attributes). In addition to his teaching and research duties at the University of Oklahoma, he leads short courses on attributes for SEG and AAPG. He currently serves as deputy editor of the SEG/AAPG publication *Interpretation*. His primary research interests include the development and calibration of new seismic attributes to aid in seismic processing, seismic interpretation, and reservoir characterization. His recent work has focused on applying coherence, spectral decomposition, structure-oriented filtering, and volumetric curvature to mapping fractures and karst with a particular focus on resource plays.